Space Sci Rev (2007) 132: 189–202
DOI 10.1007/s11214-007-9284-1

The Origin of Mercury

W. Benz · A. Anic · J. Horner · J.A. Whitby

Received: 9 February 2007 / Accepted: 2 October 2007 / Published online: 8 November 2007

Abstract Mercury's unusually high mean density has always been attributed to special circumstances that occurred during the formation of the planet or shortly thereafter, and due to the planet's close proximity to the Sun. The nature of these special circumstances is still being debated and several scenarios, all proposed more than 20 years ago, have been suggested. In all scenarios, the high mean density is the result of severe fractionation occurring between silicates and iron. It is the origin of this fractionation that is at the centre of the debate: is it due to differences in condensation temperature and/or in material characteristics (e.g. density, strength)? Is it because of mantle evaporation due to the close proximity to the Sun? Or is it due to the blasting off of the mantle during a giant impact?

In this paper we investigate, in some detail, the fractionation induced by a giant impact on a proto-Mercury having roughly chondritic elemental abundances. We have extended the previous work on this hypothesis in two significant directions. First, we have considerably increased the resolution of the simulation of the collision itself. Second, we have addressed the fate of the ejecta following the impact by computing the expected reaccretion timescale and comparing it to the removal timescale from gravitational interactions with other planets (essentially Venus) and the Poynting–Robertson effect. To compute the latter, we have determined the expected size distribution of the condensates formed during the cooling of the expanding vapor cloud generated by the impact.

We find that, even though some ejected material will be reaccreted, the removal of the mantle of proto-Mercury following a giant impact can indeed lead to the required long-term fractionation between silicates and iron and therefore account for the anomalously high mean density of the planet. Detailed coupled dynamical–chemical modeling of this formation mechanism should be carried out in such a way as to allow explicit testing of the giant impact hypothesis by forthcoming space missions (e.g. MESSENGER and BepiColombo).

Keywords Mercury: origin · Planets: formation · Numerics: simulation

W. Benz (✉) · A. Anic · J. Horner · J.A. Whitby
Physikalisches Institut, University of Bern, Sidlerstrasse 5, 3012 Bern, Switzerland
e-mail: wbenz@space.unibe.ch

J. Horner
Astronomy Group, The Open University, Walton Hall, Milton Keynes MK7 6AA, UK

1 Introduction

The density of Mercury, mean density 5.43 g/cm^3 (Anderson et al. 1987), uncompressed mean density ∼5.3 g/cm^3 (Cameron et al. 1988), is anomalously high. For comparison we note that the uncompressed mean density of the Earth is just ∼4.45 g/cm^3 (Lewis 1972). From this Urey (1951, 1952) noted that Mercury must have an iron-to-silicate ratio much larger than that of any other terrestrial planet. The silicate-to-iron mass ratio is usually estimated to lie in the range from 30 : 70 to 34 : 66 or roughly 0.5. Harder and Schubert (2001) argued that the presence of sulfur in the core could lead to even smaller ratios and that a planet entirely made of FeS could not be excluded. All of these ratios are many times smaller than those of any of the other terrestrial planets or the Moon.

A variety of hypotheses have been suggested to account for the anomalously high mean density of Mercury. In all cases, the close proximity of Mercury to the Sun plays a crucial role and all theories invoke processes that result in some level of fractionation between iron and silicates during the very early phases of the solar system in order to explain this strange mean density. Amazingly, all these scenarios and ideas date back some 20 years or more. As far as the origin of the planet is concerned, very little new work has been carried out during the last two decades. In our opinion, this reflects more the lack of new relevant data than a lack of interest in the origin of this end member of the solar system. Although new ground-based observations of Mercury have been made since the Mariner 10 mission (Sprague et al. 2007), these have not yielded a consensus on the detailed geochemical and geophysical parameters necessary to distinguish between models of Mercury's formation. It is clear that with the two new space missions dedicated to study Mercury in unprecedented detail (NASA's MESSENGER and ESA's BepiColombo; see e.g. Balogh et al. (2007)), this situation is about to change drastically. It is therefore critical to revisit the problem of the origin of Mercury and to work out models that make testable predictions in order to prepare the necessary framework in which to discuss the measurements the two future missions will be able to carry out.

Mercury formation models which have been proposed to account for this anomaly can be classified into two broad categories according to the time at which the fractionation occurs. In the first category, we find models that explain the anomalous composition of the planet as a result of fractionation that occurred during the formation of the planet proper. The second set of models encompasses those for which the planet forms first with roughly chondritic abundances and fractionates shortly thereafter. We shall briefly review these two categories in Sect. 2.

Studying Mercury's origin involves studying the dynamics and chemistry of the protoplanetary nebula in close proximity to the star. Since planets grow through collisions, the study of the formation of Mercury is also an investigation of these processes in a region where these collisions are particularly violent. Although the details of the study may be specific to just this planet, it holds implications for the formation of rocky planets (or the cores of giant planets) in general, and may provide a means for choosing between different theories.

2 The Formation of Mercury: Scenarios and Ideas

In this section we briefly recall the different scenarios that have been proposed to explain Mercury's anomalous composition. In all the currently available scenarios, the main point is to achieve enough chemical fractionation to account for the high density of the planet. Not

surprisingly, all these scenarios take place very early on in the history of the solar system either as an ongoing process during the formation of the planets, or during the late stages of accretion or shortly thereafter. They all rely in some way on the peculiar position of the planet, namely its close proximity to the Sun.

2.1 Fractionation During Formation

In this class of models, the anomalous density of Mercury results from fractionation occurring during the formation process itself. In its simplest form, fractionation is obtained as a result of an equilibrium condensation process in a proto-planetary nebula in which the temperature is a monotonic function of the distance to the Sun (Lewis 1972, 1974; Barshay and Lewis 1976; Fegley and Lewis 1980). Such models predict that the condensates formed at Mercury's distance were both extremely chemically reduced and extremely poor in volatiles and FeO. Metallic iron would be partially condensed while refractory minerals rich in calcium, aluminum, titanium and rare earths would be fully condensed. The bulk average density of the condensed material would therefore be much higher in the Mercury region than in the formation regions of the other terrestrial planets hence explaining the high mean density.

Although such simple models of the chemical behavior of the solid material in the early solar nebula successfully predict some of the most general compositional trends of solar system bodies, it was recognized by Goettel and Barshay (1978) and later by Lewis (1988), that this mechanism cannot explain the anomalous density of Mercury. The main reason for the failure of this model is the relatively small difference in the condensation temperature of core and mantle material. This implies also a close spatial proximity in the nebula while the area over which the material must be collected to actually bring a planetary mass together, is much larger. The high-density material is simply diluted with lower density material. Lewis (1988, and references therein) showed that this results in a maximum core mass fraction of about 36% as compared to the 70% for the actual planet. Hence, simple condensation–accretion models fail to explain the mean density of Mercury.

To circumvent these difficulties, various additional fractionation mechanisms operating during, or even before, the start of planetary accretion have been proposed. While some combination of these mechanisms based on microscopic differences between silicates and iron (ferromagnetism, strength, etc.) may possibly lead to higher mean densities, there exist no compelling reasons why these mechanisms should have been more active at Mercury than other places in the solar system (see Weidenschilling 1978 for a detailed discussion). Weidenschilling (1978), on the other hand, proposed that the additional fractionation results from a combination of gravitational and drag forces. As the early condensates orbited the Sun, immersed in a gaseous disk, they felt a drag force that depends in a complex fashion upon the size and shape of the condensed particles and upon the structure of the nebula. As a result of this drag force, orbiting bodies lose angular momentum and spiral inward. In a simple quantitative model, Weidenschilling (1978) showed that the rate of orbital decay is slower for larger and/or denser bodies. With suitable but reasonable assumptions for the initial conditions, Weidenschilling (1978) showed that the fractionation required to produce iron-rich planets can be achieved.

Following the three-dimensional dynamics of a dusty gas over periods of time vastly exceeding a dynamical timescale is a complicated problem, especially since the dynamics of the gas itself is still up for debate. For example, the origin of the turbulence, the existence of instabilities, the presence of spiral waves, among others, are still unclear. Hence, short of a better understanding of the dynamics of this multicomponent fluid, it is difficult to assess to

what extent models based on fractionation occurring in a laminar nebula before and during planet formation are realistic.

2.2 Fractionation after Formation

Cameron (1985) proposed that, during the early evolution of the solar nebula, temperatures at the position of Mercury were probably in the range 2,500–3,000 K. If a proto-Mercury existed at the time, partial volatilization of the mantle would occur thus creating a heavy silicate atmosphere which could over time be removed by a strong solar wind. Fegley and Cameron (1987) computed the expected bulk chemical composition of the mantle as a function of evaporated fraction using both ideal and nonideal magma chemistry. They showed that starting with a proto-Mercury of chondritic abundance (2.25 times the mass of the present day planet) Mercury's mean density can be obtained after 70–80% of the mantle has evaporated. At this point, the remaining mantle is depleted in the alkalis, FeO and SiO_2, but enriched in CaO, MgO, Al_2O_3 and TiO_2 relative to chondritic material. Fegley and Cameron (1987) argued that this anomalous composition represents a unique signature of this formation scenario that could eventually be measured by a dedicated spacecraft mission.

This scenario has the clear advantage of having its consequences calculated in enough detail to allow potentially explicit testing. However, it also suffers from a number of difficulties. For example, it is not clear whether high enough temperatures can be reached and maintained for long enough in the solar nebula *after* a suitable proto-Mercury has been formed. Furthermore, as already identified by Cameron (1985) himself, the solar wind may not be efficient enough to remove the heavy silicate atmosphere thus preventing a significant evaporation of the mantle.

In another scenario to explain Mercury's anomalous density, the removal of a large fraction of the silicate mantle from the originally more massive proto-Mercury is achieved following one (or possibly more) giant impacts (Smith 1979; Benz et al. 1988; Cameron et al. 1988). In this hypothesis, a roughly chondritic Mercury (2.25 times the mass of present day Mercury) is hit by a sizable projectile (about 1/6 its mass in the calculations by Benz et al. 1988) at relatively high velocity. Such an impact results in the loss of a large fraction of the mantle leaving behind essentially a bare iron core (see Sect. 3). The existence of large projectiles was first suggested by Wetherill (1986), who realized that terrestrial proto-planets probably suffered collisions with bodies of comparable mass during the final stages of their formation. He also proposed that the high relative velocities in Mercury's formation region could lead to particularly disruptive collisions making the formation of Mercury unique among the terrestrial planets.

Simulations (Benz et al. 1988; Cameron et al. 1988) have shown that the required removal of the silicate mantle can be achieved by a giant impact. However, the question of the long-term fate of the material ejected from such an impact has never been properly investigated. Indeed, most of the ejected material following the impact is still orbiting the Sun on Mercury crossing orbits and will therefore eventually collide with the planet and be reaccreted over time unless it is removed by some other processes. If a significant fraction should indeed be reaccreted, the fractionation obtained as a result of the collision would only be short lived and therefore would not explain the present-day mean density of the planet.

Both gravitational scattering and the Poynting–Robertson effect have been invoked as possible ejecta-removal mechanisms. However, the former is found to remove only a very small amount of material (see Sect. 4.1) and the efficiency of the second depends on the size distribution of the ejecta. Simple condensation models based on equilibrium thermodynamics (Anic 2006) show that the expanding vapour cloud following the impact would

lead to the formation of small-sized condensates (see Sect. 4.1). These small-sized condensates can readily be affected by nongravitational forces such as those originating from the Poynting–Robertson effect. Hence, from a dynamical point of view, the giant impact scenario as proposed by Benz et al. (1988) and Cameron et al. (1988) appears to be possible. It remains to be determined, however, whether the chemical signature of such a giant impact is compatible with the bulk chemistry of Mercury.

3 Simulations of Giant Impacts

3.1 Initial Conditions

As the target body in our collision simulations, we adopt a proto-Mercury that has roughly chondritic abundance. We built such a proto-Mercury by increasing the mass of the silicate mantle of the planet until the present-day core mass represents only about 1/3 of the planet's total mass. With this structure, the total mass of proto-Mercury amounts to 2.25 times the mass of present-day Mercury. Its internal structure is computed using the usual equations assuming an adiabatic temperature profile (Spohn et al. 2001). For the equation of state (EOS) in our calculations we use ANEOS (Thompson and Lauson 1984). This analytical EOS relates temperature and density to pressure, and describes mixed states (liquid–vapour, solid–vapour) using the Helmholtz free energy potential. The equation requires 24 coefficients for a given material which, for the most part, can be derived from laboratory experiments. We assume that the mantles of the projectile and the target consist of dunite (a rock consisting largely of forsteritic olivine Mg_2SiO_4) which has similar bulk properties to mantle rock. The table of parameters for dunite was given by Benz et al. (1989). The core of the planet is assumed to consist of pure iron.

Finally, we must specify boundary conditions and in particular the value of the temperature at the surface of the planet and the projectile. Since this value is not known at the time of formation of the planet, we use two different values which should bracket the possibilities reasonably well. In one case, we use the present-day mean surface temperature of 452 K and for the other we consider a much hotter body with a surface temperature of 2,000 K. We shall refer to these two models in the text as *cold* and *hot*.

3.2 Numerics and Model Assumptions

Following Benz et al. (1988), we use a 3D Smooth Particle Hydrodynamics (SPH) code to simulate the impacts. SPH is a Lagrangian method in which the motion of the mass elements (particles) is followed over time. Given that SPH has already been described many times in the literature and that we use a fairly standard implementation of the method, we refer the reader to reviews by Benz (1990) and Monaghan (1992) for further detailed explanation of the method. In the present work, we use the version of SPH described by Benz (1990), with only a small number of modifications. The major change is the use of individual artificial viscosity coefficients that vary over time using the shock detection algorithm proposed by Morris and Monaghan (1997), which minimises the viscosity outside shocks.

In all cases, we neglected the strength of the material. This assumption is reasonable given the size of the bodies involved for which self-gravity and pressure gradients are the dominating forces. Self-gravity is computed using a hierarchical binary tree as discussed by Benz (1990). We also neglect radiative losses during the impact (cooling due to adiabatic

expansion is included). The main reason for this is to avoid the considerable additional numerical work that would be needed to compute such radiative losses. From a physical point of view, the assumption is justified by the fact that the simulations proper extend only over a relatively short amount of real time during which the radiative losses should remain small. We investigated simple models of radiative cooling as part of the condensation calculations presented in Sect. 4.1.

The simulations were carried out until the ultimate fate of the material could be reliably determined. At that time, we identified the material having being lost by the planet using the same iterative procedure (based on binding energy) as described by Michel et al. (2002). For the material remaining gravitationally bound, we compute the fractions of silicate and iron in order to determine the rock-to-iron (R/I) ratio.

3.3 Results

We performed a number of simulations of giant collisions with different projectile masses, impact velocity and impact geometries in order to find collisions that lead to a suitable fractionation. However, we did not carry out an extensive search to find all the possible initial conditions leading to the desired result. Hence, we cannot compute the actual probability of such an event. However, we note that success (see Table 1) does not involve exceptional geometries or mass ratios. On the other hand, the velocity at which the two large bodies must collide in order to ensure almost complete mantle loss is relatively high. Such high relative velocities are much more likely to occur in the inner regions of the solar system

Table 1 Simulations involving the "cold" (runs 1–12) and "hot" (runs 13–17) proto-Mercury

Run	b [R]	$v_{\rm rel}$ [km/s]	$m_{\rm imp}/m_{\rm tar}$	$N_{\rm p}$	$N_{\rm t}$	R/I	M_f
1	0.7	30	0.1	11′326	113′129	1.32	1.73
2	0.5	27	0.1	15′543	155′527	1.10	1.50
3	0	20	0.1	11′326	113′129	1.25	1.63
4	0.5	26	0.167	23′556	141′392	0.78	1.18
5	0.53	28	0.167	23′556	141′392	0.59	1.01
6	0	20	0.167	23′556	141′392	0.61	0.92
7	0	26	0.167	23′556	141′392	0.11	0.15
8	0.7	26	0.2	49′485	247′423	1.11	1.52
9	0.7	28	0.2	28′269	141′392	0.94	1.38
10	0.6	30	0.2	27′411	137′200	0.51	0.94
11	0.5	28	0.2	27′411	137′200	0.50	0.86
12	0	28	0.2	27′411	137′200	–	0
13	0.47	23	0.167	21′205	127′249	0.87	1.27
14	0.5	24	0.167	21′205	127′249	0.86	1.26
15	0	19	0.2	28′269	141′392	0.71	1.01
16	0.46	25.5	0.2	28′269	141′392	0.51	0.87
17	0.5	28	0.2	28′269	141′392	0.49	0.85

$N_{\rm p}$ is the number of particles in the projectile and $N_{\rm t}$ in the target. The impact parameter b is given in units of target radius and the relative velocity is given in km/s. R/I is the silicate to iron ratio in the surviving planet and M_f is its final mass in units of present-day Mercury mass. The planet in run 12 disintegrated

where the Keplerian velocities are already large. Hence, extreme collisional fractionation of full-grown planets can, from a theoretical point of view, involve only planets orbiting deep in the potential well. This is consistent with the fact that Mercury is the only planet in the solar system with such a high mean density.

The initial conditions for the simulations performed and the final characteristics of the surviving planets are given in Table 1. Note that some of the runs are very similar to those performed by Benz et al. (1988) but with a considerable increase in the number of particles used (typically 20 to 50 times more).

In the various cases listed in this table, the collisions leading to a final mass of $M_f \approx 1$ (in units of present day Mercury mass) and a silicate to iron mass ratio $R/I = 0.4$–0.6 can be considered as successful in the sense that they reproduce the bulk characteristics of present-day Mercury. In fact, depending upon the subsequent reaccretion of a fraction of the silicate mantle (see Sect. 4), simulations with R/I less than the present-day value should be considered as successful.

Note that, in order to remove a sizable fraction of the silicate mantle, the collision speed must be quite high, especially in the case of an off-axis collision for which the strength of the shock is significantly weaker (all other parameters being equal). Statistically, the most probable collisions are those with $b = 0.7 R_{\text{proto-Mercury}}$ (Shoemaker 1962) where the impact parameter b is defined as the distance from the centre of the target to the centre of the impactor along a line normal to their relative velocity (b is thus zero for a head-on collision and $R_{\text{proto-Mercury}} + R_{\text{impactor}}$ for a grazing collision). However, for realistic relative velocities and reasonable-sized projectiles, these dynamically most probable collisions seem not to result in a large enough loss of mantle material.

Overall, the simulations that appear to yield potentially satisfactory results are runs 6, 10, 11 in the case of a "cold" proto-Mercury and runs 16, 17 for the "hot" progenitor. Hence, as far as the initial blasting off of the mantle is considered, the thermal state of the progenitor does not appear to play a major role. Collisions involving "hot" bodies are not overwhelmingly more disruptive that those involving "cold" ones. In fact, similar results can be obtained by relatively small changes in collision characteristics. To illustrate a typical collision, Fig. 1 shows a set of four snapshots illustrating run 11.

We note how severe this collision actually is. The planet is nearly destroyed in the process and it is actually gravitational reaccumulation that brings the core of the planet back together. Such nearly destructive collisions are required if most of the mantle of a roughly chondritic proto-Mercury is to be removed. This also shows that destroying *large* bodies by means of collisions is not so easy and requires large impactors and high velocities. We argue that this implies that such events can only occur in regions near the star where the collision velocities can be high enough. If this is correct, it could explain why only Mercury fractionated to such an extent even though all the other terrestrial planets also experienced giant collisions during their formation. This makes Mercury particularly important for the study of terrestrial planet formation. We also note that as a result of the severity of the impact, all the material reaches high temperatures and thus the assumption made by Harder and Schubert (2001), that a Mercury formed by means of a giant impact could have a volatile rich composition and lose more iron than sulfur during the collision, seems unlikely to be true.

Finally, we point out that our run 5 had almost identical initial conditions to run 13 by Benz et al. (1988) and that the outcomes are very similar even though in this work we have been able to use about 50 times as many particles!

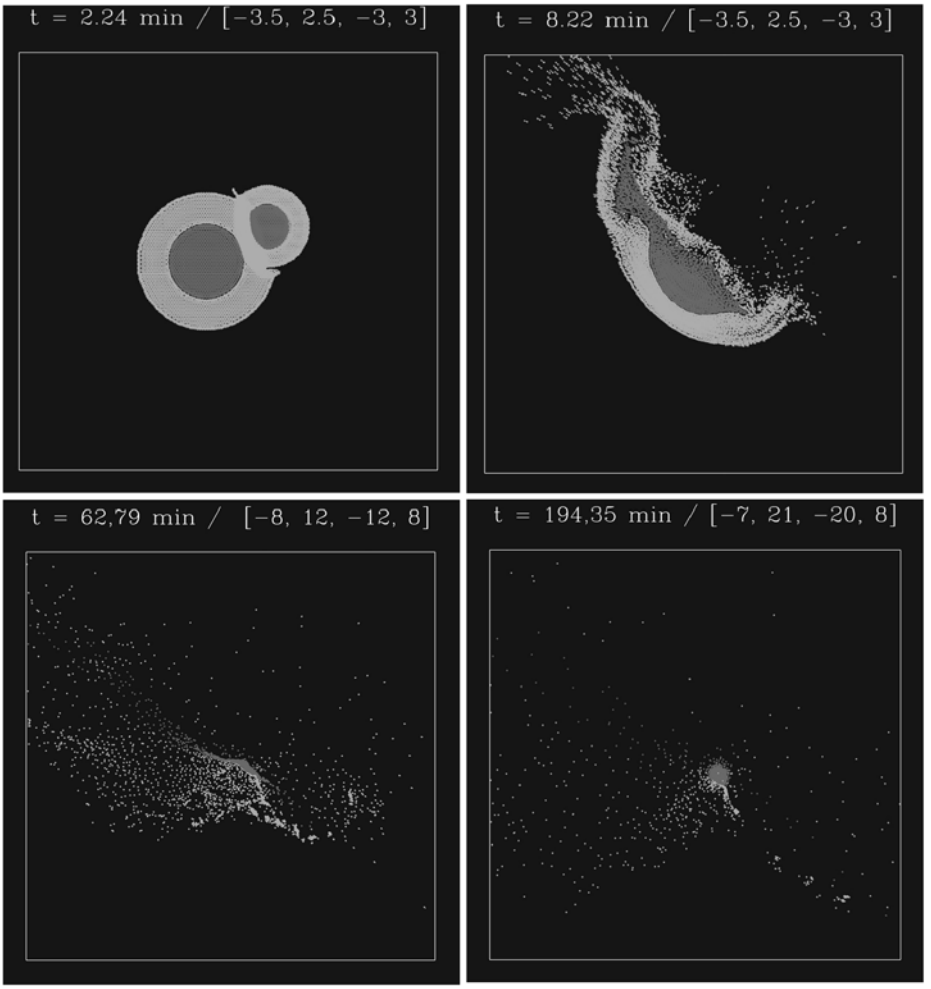

Fig. 1 Snapshots from the evolution of run 11. Particles in a slice running through the central plane are plotted. Velocity vectors are normalized to the maximum vector in each figure and plotted at particle locations. Iron is shown in *dark grey*, whilst *light grey* represents silicates. The time after first contact (in minutes), along with the coordinates of the quadrant given in units of target radius, is given above each snapshot

4 The Fate of the Ejecta

As mentioned in Sect. 1, a giant impact removes most of the rocky mantle is not sufficient to explain the present-day bulk composition of Mercury. It is also necessary to demonstrate that the overwhelming part of the ejected matter is not reaccreted by the planet over time. For this to happen, it needs to be removed from Mercury crossing orbits before it collides with the planet again. In order to address these issues, we first computed the size distribution of the ejected matter (Sect. 4.1) and then compared the timescale required by the Poynting–Robertson effect to remove the ejecta (Sect. 4.2) with the timescale until collision with the planet (Sect. 4.3). We also investigated how effective gravitational torques exerted by other planets can be in ejecting the material (Sect. 4.3).

4.1 Size Distribution of the Ejecta

To compute the final size distribution of the ejected matter it is necessary to follow its thermodynamical evolution. This is conveniently done by using a $T-\rho$ diagram such as that sketched in Fig. 2. In our calculations we assume equilibrium thermodynamics, neglecting all rate-dependent effects. To check the importance of the equation of state, we computed the cooling curves using both a perfect gas EOS and ANEOS. For simplicity, but partially justified by the short duration of the impact, we also omit radiative losses and assume that the internal energy of the hot gas is entirely transformed into the kinetic energy of the expansion. Finally, in following the ejected matter, we treat each SPH particle as an independent piece of material ignoring the potential interactions (heat exchange, collisions, etc.) between the expanding particles. The overall size distribution is obtained by summing up the distributions obtained for all ejected SPH particles.

Upon being struck by a very large, fast-moving body, a large fraction of the target material is compressed to extreme pressures at which both metallic and siliceous liquids exhibit characteristics of a supercritical fluid ("hot vapour" in what follows). The path followed by the material during this compression phase is shown by ① in Fig. 2. During the subsequent very rapid decompression of the compressed liquid and the expansion of the hot vapour the matter undergoes a phase transition from either the liquid or the vapour side of the vapour-liquid dome (respectively ② and ③ in Fig. 2). Depending upon the cooling path taken by the hot vapour, we use two different approaches to compute the size distribution of the condensates following the phase transition.

In the case that the transition occurs along path ③, we use the homogenous condensation model of Raizer (1960). In this model, when the expanding vapour cloud crosses the vapour–liquid boundary given by the Clausius–Clapeyron equation, the vapour enters first a

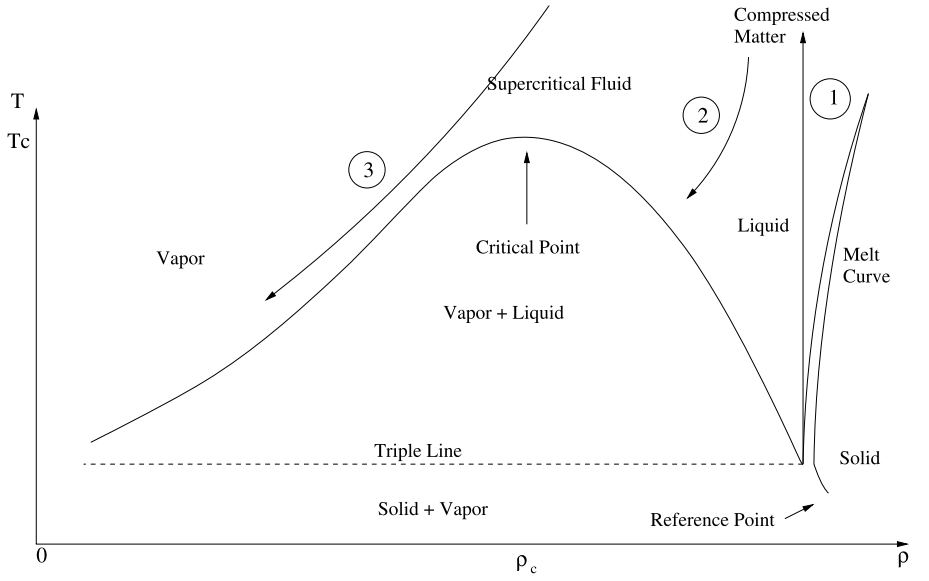

Fig. 2 Schematic T, ρ vapour–liquid–solid diagram. T_c and ρ_c indicate the critical point above which one cannot separate liquid from vapour. The reference point points to room-temperature conditions. The matter is shocked along path ①, and relaxed along the paths ② and ③

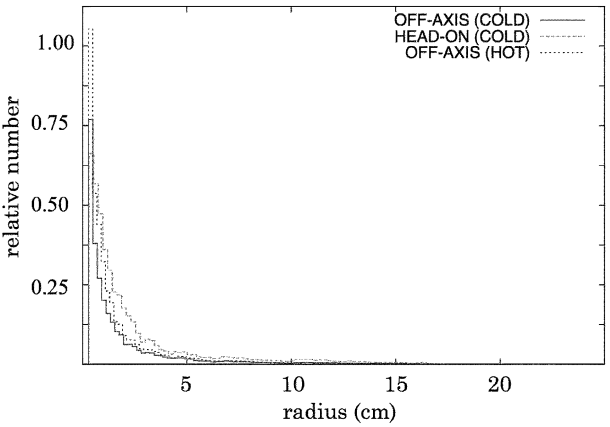

Fig. 3 Size distribution of particles (condensates and melt droplets) which result from runs 6, 11 and 17 using ANEOS. Particle sizes range from 1.7×10^{-6} cm to 22.3 cm for run 6, 1.6×10^{-6} cm to 21.4 cm for run 11, and from 1.6×10^{-2} cm to 20.7 cm for run 17

saturated and then a supersaturated (metastable) state. The vapour then undergoes a partial transformation into liquid droplets, where each droplet contains some average number of atoms. Their growth is only possible if their volume energy exceeds their surface energy. The number of liquid droplets formed is given by the nucleation rate which depends critically upon the surface tension σ. In our calculations we adopt $\sigma = 1{,}400$ erg/cm^2 for iron (Gail and Sedlmayr 1986) and $\sigma = 350$ erg/cm^2 for dunite (Elliot et al. 1963). It is beyond the scope of this paper to discuss this model in more detail, but the interested reader will find more in the original paper and in Anic et al. (2007).

On the other hand, if the hot vapour cools along path ②, we use the formalism provided by Grady (1982) to compute the decompression and fragmentation. We also check whether droplet formation is governed by dynamic fragmentation (Grady 1982) or the liquid to vapour transition (Melosh and Vickery 1991), or both. Here again we refer the reader to the original papers and to Anic et al. (2007) for more details.

The resulting distributions of droplet sizes obtained for runs 4 (head-on, "cold"), 11 (off-axis, "cold") and 17 (off-axis, "hot") are shown in Fig. 3.

For all three runs, the majority of the droplets are less than 5 cm in radius with a peak at or slightly below 1 cm. The differences between the three simulations, as far as the size distribution is concerned, are relatively small. Results obtained using a perfect gas EOS to compute the expansion lead to somewhat smaller condensates. In particular, the peak of the distribution is markedly below 1 cm. We conclude that giant impacts that lead to a suitable fractionation of a chondritic proto-Mercury produce essentially centimeter and subcentimeter sized particles in the ejecta.

4.2 Non-gravitational Forces

Several nongravitational mechanisms may perturb the orbit of dust particles. Because we assume that both our proto-Mercury and the impactor are quite large and have differentiated to form iron cores, we may presume that the impact occurs late enough that the nebular gas has dissipated. We may therefore neglect the effect of gas drag on the ejecta; drag due to the modern solar wind is significant only for particles of size less than one micron. Because the overwhelming majority of the condensates and (solidified) melt droplets are less than 1 cm in size, we may also neglect the Yarkovsky effect (see e.g. Bottke et al. 2000). We are left

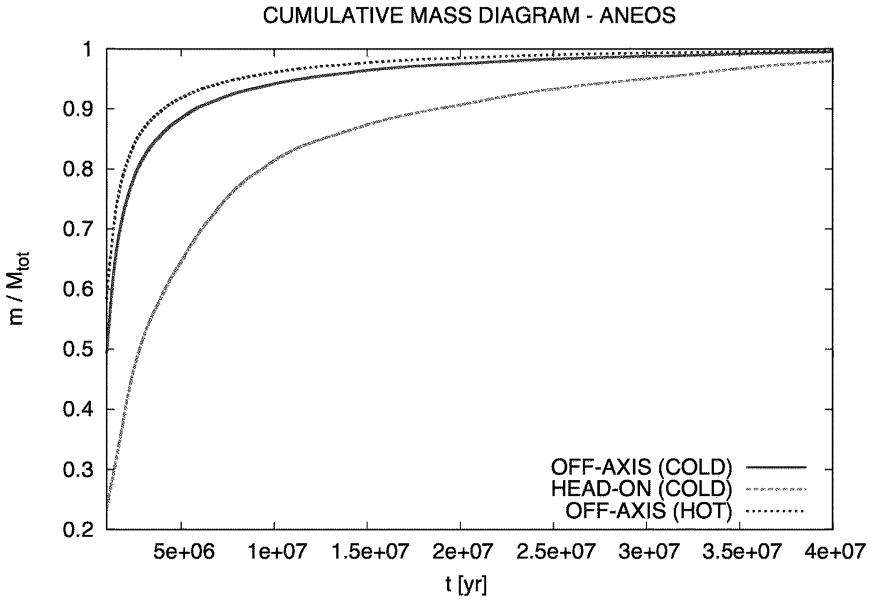

Fig. 4 The effect of Poynting–Robertson drag on particles with initial orbits and particle sizes determined from our SPH simulations and condensation calculations. Results for three different impact scenarios are shown, and the ANEOS equation of state was used in all cases. The figure shows the mass fraction of ejecta particles collected by the Sun as a function of time after the impact. In the slowest case, for a head-on impact with a cold proto-Mercury, the half-life of the particles is about 2.5 Myr

with direct photon pressure and the Poynting–Robertson effect. For particles of the densities considered here, the Poynting–Robertson effect is dominant for particle sizes greater than 1 micron.

Poynting–Robertson drag arises from the relativistic interaction of dust particles with solar photons. Robertson (1937) investigated the fate of small particles in circular orbits and set up the corresponding equations of motion. Wyatt and Whipple (1950) extended the method to the general case of elliptic orbits. Using the equations published in those papers we can calculate the time scales on which the condensates (and melt droplets) resulting from the simulations presented earlier disappear into the Sun.

Knowing the size distribution of the ejecta and knowing the corresponding material density, we need only the initial orbital elements of the condensates in order to actually compute their removal timescale. We obtain these orbital elements for each ejected SPH pseudo-particle by picking an arbitrary impact site somewhere along proto-Mercury's orbit which gives us the centre of mass velocity to which we add the ejection velocity as computed by the hydrodynamics code. We further assume that all particles are spherical and of uniform density and that they intercept radiation from the Sun over a cross-section πr^2 and isotropically reemit it at the same rate (thermal equilibrium). The relevant decay equations for this case can be found in Wyatt and Whipple (1950) and Fig. 4 shows the results of applying these equations to the simulated ejecta particles. For simplicity we have neglected the effects of finite size and rotation of the Sun (Mediavilla and Buitrago 1989). The time-scale for removal of particles with our calculated size distribution can be seen to be less than a few million years.

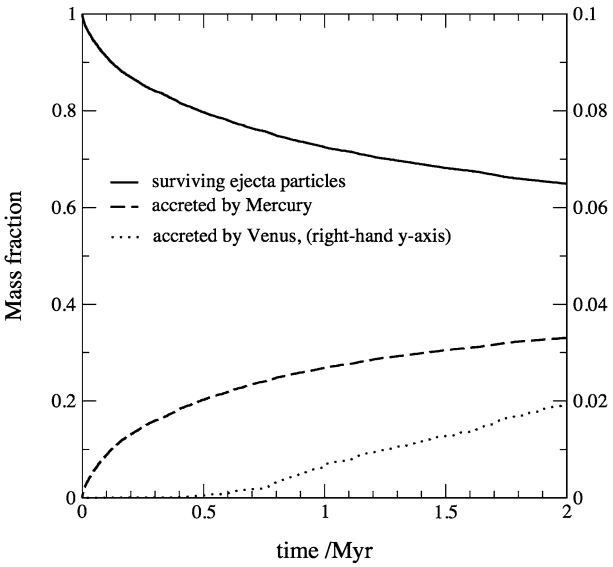

Fig. 5 Decay of a population of particles ejected from Mercury in a head-on collision (simulation run 6) at the perihelion of the planet's orbit. N.B. the fraction of particles colliding with Venus has been scaled up for better visibility

4.3 Collision Time and Gravitational Scattering

The ejecta from the collision initially have heliocentric orbits which still cross the orbit of Mercury. Unless they are removed from such orbits, e.g. by the Poynting–Robertson effect (see Sect. 4.2) or by gravitational scattering, most of the matter will be reaccreted by the planet over time and the resulting collisional fractionation will be too small to explain the planet's anomalous composition.

In order to study the dispersal and reaccretion of the ejected matter under the effects of gravity, a number of simulations were carried using the hybrid integrator MERCURY (Chambers 1999). We simulated the behaviour of a large population of ejected particles under the gravitational influence of Mercury (taken as being the mass of the currently observed planet), Venus, Earth, Mars and Jupiter, for a period of two million years. For lack of a better choice, these planets were placed on their current orbits. The ejected particles were treated as being massless, and were followed until they were either ejected from the inner Solar system (passing beyond the orbit of Jupiter), or collided with one of the planetary bodies. Their initial positions and velocities were computed using hermeocentric velocities chosen randomly from amongst the ejected SPH pseudo-particles, the choice of a position of proto-Mercury on its orbit at the time of the impact and the necessary coordinate transformation from a hermeocentric to a heliocentric frame of reference.

Two different series of integrations were run. The first simulation, which was the most detailed, followed the behaviour of 10,000 ejected particles over the two million year period for the case of a head-on collision. The second series of simulations used a smaller dataset (1,000 particles), but examined the effect of the collision location, the collision geometry (head-on vs. glancing, as described earlier) and the effect of scaling the mass of the remnant planet. Here we show only the results from the simulation involving the large number of particles (Fig. 5). The other simulations yield very similar results except for when the collision occurs at aphelion; in this case the rate of reaccretion is significantly less.

It can clearly be seen from Fig. 5 that the number of surviving particles decays over time, with the bulk of the removed material being lost to reaccretion by Mercury. However, the

rate at which material reaccretes is particularly low—after two million years, 6,496 of the 10,000 particles remain in the simulation, which corresponds to a decay half-life of about 3.2 Myr. Of the 3,504 particles which were removed from the simulation over the course of the 2 million year period, 3,306 were reaccreted by Mercury, while 191 hit Venus, with the remaining 7 particles hitting the Sun or being ejected beyond the orbit of Jupiter. In longer simulations, particles were observed to impact the Earth, and an ever-increasing fraction were ejected from the system rather than being accreted, so it is clear that the particles slowly diffuse throughout the inner Solar system as a result of repeated encounters with the inner planets. These results are consistent with those obtained by Gladman (2003) for slightly different initial conditions. Warrel et al. (2003) found that hermeocentric and 1:1 Mercury mean motion resonance orbits can be stable for long time periods, but that ejecta with velocities only slightly greater than the escape velocity are likely to be reaccreted due to the necessity of successive close encounters with Mercury to achieve significant gravitational scattering. They did not, however, provide a numerical result.

In Sect. 4.2 we showed that the half-life of the condensates is of order 2.5 Myr before they are removed by the Poynting–Robertson effect. Over the same period of time, roughly 40% of particles are found to collide with Mercury. This implies that successful collisions are really those for which the post-collision R/I ratio is somewhat less than Mercury's present-day ratio probably in the range $0.3 \leq R/I \leq 0.4$ in order to allow for this reaccretion. No attempt was made to simulate a collision that would, after reacculation, lead to the exact R/I ratio. However, since our ratios bracket the desired value there would be no problem to find an appropriate collision. We conclude that giant collisions as envisioned here can indeed lead to significant long-term chemical fractionation.

5 Summary and Conclusions

We have confirmed, using SPH models with a significantly higher resolution than previous efforts, that a giant impact is capable of removing a large fraction of the silicate mantle from a roughly chondritic proto-Mercury. The size and velocity of the impactor were chosen to be consistent with predictions of planetary formation and growth, and a plausible Mercury can be obtained for several assumptions about initial temperatures and impact parameter.

We extended the previous work on the subject by addressing the fate of the ejecta in order to assess the fraction that could be reaccumulated by Mercury thereby changing again the fractionation achieved immediately after the impact. In particular, using a simple condensation model, we derived the expected size distribution of the ejected material after it cools following adiabatic expansion, and the subsequent dynamical evolution of the resulting particles. The loss of ejected particles into the Sun due to Poynting–Robertson drag was shown to be at least as efficient as reaccretion onto Mercury, and so the bulk density and composition that result from the giant impact would have been largely retained. The giant impact hypothesis for the formation of Mercury is thus entirely plausible.

Our simulations provide estimates of particle size and temperature, and gas density in the ejecta plume. First-order estimates of chemical mixing and loss of volatile elements could perhaps be undertaken with this information. Future simulations will concentrate on chemical fractionation resulting from the impact, and may have sufficient resolution to consider the effect of large ion lithophiles having been preferentially incorporated into a "crust" on the proto-Mercury. These more sophisticated simulations would then be able to make predictions about the isotopic and elemental composition of the modern Mercury. These predictions could then be tested, at least in part, by the data expected from the two coming Mercury spacecraft missions.

Confirming the collisional origin of the anomalous density of Mercury would go a long way toward establishing the current model of planetary formation through collisions which predicts giant impacts to happen during the late stages of planetary accretion. Hence, small Mercury has the potential to become a Rosetta stone for the modern theory of planet formation!

Acknowledgements The authors gratefully acknowledge partial support from the Swiss National Science Foundation.

References

J.D. Anderson, G. Colombo, P.B. Esposito, E.L. Lau, G.B. Trager, Icarus **71**, 337 (1987)
A. Anic, PhD Thesis, University of Bern, 2006
A. Anic, W. Benz, J. Horner, J.A. Whitby, Icarus (2007, in preparation)
A. Balogh, R. Grard, S.C. Solomon, R. Schulz, Y. Langevin, Y. Kasaba, M. Fujimoto, Space Sci. Rev. (2007, this issue). doi:10.1007/s11214-007-9212-4
S.S. Barshay, J.S. Lewis, Annu. Rev. Astron. Astrophys. **14**, 81 (1976)
W. Benz, in *The Numerical Modelling of Nonlinear Stellar Pulsations Problems and Prospects*, ed. by J.R. Buchler (1990), p. 269
W. Benz, A.G.W. Cameron, W.L. Slattery, Icarus **74**, 516 (1988)
W. Benz, A.G.W. Cameron, H.J. Melosh, Icarus **81**, 113 (1989)
W.F. Bottke, D.P. Rubincam, J.A. Burns, Icarus **145**, 301 (2000)
A.G.W. Cameron, Icarus **64**, 285 (1985)
A.G.W. Cameron, B. Fegley, W. Benz, W.L. Slattery, in *Mercury*, ed. by F. Vilas, C. Chapman, M.S. Matthews (University of Arizona Press, Tucson, 1988), 692 pp
J.E. Chambers, Mon. Not. R. Astron. Soc. **304**, 793 (1999)
J.F. Elliot, M. Gleiser, V. Ramakrishna, in *Thermochemistry for Steelmaking*, vol. II (Addison-Wesley, 1963)
B. Fegley Jr., A.G.W. Cameron, Icarus **82**, 207 (1987)
B. Fegley Jr., J.S. Lewis, Icarus **41**, 439 (1980)
H.P. Gail, E. Sedlmayr, Astron. Astrophys. **166**, 225 (1986)
B. Gladman, LPSC **XXXIV**, #1933 (2003)
K.A. Goettel, S.S. Barshay, in *The Origin of the Solar System*, ed. by S. Dermott (Wiley, Chichester, 1978), 611 pp
D.E. Grady, J.A.P. **53**, 322–325 (1982)
H. Harder, G. Schubert, Icarus **151**, 118 (2001)
J.S. Lewis, Earth Planet. Sci. Lett. **15**, 286 (1972)
J.S. Lewis, Science **186**, 440 (1974)
J.S. Lewis, in *Mercury*, ed. by F. Vilas, C. Chapman, M.S. Matthews (University of Arizona Press, Tucson, 1988), p. 651
E. Mediavilla, J. Buitrago, Eur. J. Phys. **10**, 127 (1989)
H.J. Melosh, A.M. Vickery, Nature **350**, 494 (1991)
P. Michel, W. Benz, P. Tanga, D. Richardson, Icarus **160**, 448 (2002)
J.J. Monaghan, Annu. Rev. Astron. Astrophys. **30**, 543 (1992)
J.P. Morris, J.J. Monaghan, J. Comput. Phys. **136**, 41 (1997)
Y.P. Raizer, J. Exp. Theor. Phys. **37**(6), 1229 (1960)
H.P. Robertson, Mon. Not. R. Astron. Soc. **97**, 423 (1937)
E.M. Shoemaker, in *Physics and Astronomy of the Moon*, ed. by Z. Kopal (Academic, New York and London, 1962)
J.V. Smith, Mineral. Mag. **43**, 1 (1979)
T. Spohn, F. Sohl, K. Wieczerkowski, V. Conzelmann, Phys. Space Sci. **49**, 1561 (2001)
A. Sprague, J. Warell, G. Cremonese, Y. Langevin, J. Helbert, P. Wurz, I. Veselovsky, S. Orsini, A. Milillo, Space Sci. Rev. (2007, this issue). doi:10.1007/s11214-007-9221-3
H.S. Thompson, S.L. Lauson, Sandia Labarotories Report SC-RR-710714 (1984)
H.C. Urey, Geochim. Cosmochim. Acta **1**, 209 (1951)
H.C. Urey, *The Planets* (Yale University Press, New Haven, 1952)
J. Warrel, O. Karlsson, E. Skoglov, Astron. Astrophys. **411**, 291 (2003)
S.J. Weidenschilling, Icarus **35**, 99 (1978)
G.W. Wetherill, in *Origin of the Moon*, ed. by W.K. Hartmann, R.J. Phillips, G.J. Taylor (Lunar and Planetary Institute, Houston, 1986), 519 pp
S.P. Wyatt Jr., F.L. Whipple, Astrophys. J. **111**, 134 (1950)